PAPER

Check for updates

A functionalized polyamide acid additive for perovskite solar cells with high efficiency and stability†

Huanting Luo,[a] Fanlin Tu,[a] Xiaotong Chen,[a] Longjiang Xing,[a] Leliang Cao,[a] Guoxing Ren,[b] Shaomin Ji, [ID][a] Yuanhong Zhong,[a] Liangang Xiao,[b] Wen-Cheng Chen, [ID][a] Qing-Dan Yang, [ID]*[a] Chen Yang [ID]*[c] and Yanping Huo [ID]*[a]

Perovskite solar cells (PSCs) have reached a certified power conversion efficiency (PCE) of 25.7% in 2022 benefiting from their high absorption coefficient, high carrier mobility, long diffusion length and tunable bandgap. However, due to the features of solution processing and rapid crystal growth of perovskite thin films, a variety of defects inevitably can form because of the precursor compositions and processing conditions. Actually, defects accumulating at the surface and grain boundaries are detrimental to both the device performance and stability of perovskite solar cells. Small molecules and polymers with functional groups have been employed to passivate the defects but suffer from complex synthesis processes and high costs. Herein, a novel polyamide acid (poly(6FDA-*co*-AHHFP); denoted as PAA) with multi-functional groups was developed by a one-pot method at room temperature and the polymer was introduced into a perovskite precursor solution as an additive to improve the perovskite film crystallinity, enlarge the grain boundaries, and passivate the defects, yielding enhanced PCE. PSCs with a 0.2 mg mL^{-1} optimized concentration of PAA exhibit a PCE of 20.03% with a high fill factor (FF) of 80.34%. In addition, the device with PAA as an additive demonstrated less hysteresis than that without an additive, as well as excellent reproducibility. Meanwhile, the device with the PAA additive also showed enhanced operational stability compared to the reference one. This work presents a novel polymer prepared by a one-pot method used as an additive in perovskite solar cells to achieve high performance and stability.

Introduction

Hybrid perovskite solar cells (PSCs) have attracted intensive attention in scientific communities and is regarded as a vital option among next-generation photovoltaics due to their high power conversion efficiency (PCE) and solution-processability and mechanical flexibility.[1–5] Since the first application of lead halide perovskite materials as a light absorption layer by Miyasaka and co-workers, the PCE has been boosted to a certified value of 25.7% compared to the initial one of 3.8%.[6] However, due to the intrinsic properties of lead halide perovskite materials, organic cations tend to escape from the perovskite crystal during the thermal annealing process, resulting in decomposition of perovskite crystals and formation of a large number of ionic defects, which serve as nonradiative recombination centers.[7–10] In addition, lead halide perovskite materials are very sensitive to ambient moisture. Although advanced encapsulation techniques have been developed to minimize the influence of suffering from extrinsic environmental factors,[11,12] the defects at the surface and grain boundaries are detrimental to the performance and stability of PSCs. Therefore, eliminating the defects and suppressing the nonradiative recombination at the bulk, grain boundaries and surface are important to the performance of PSCs.[13]
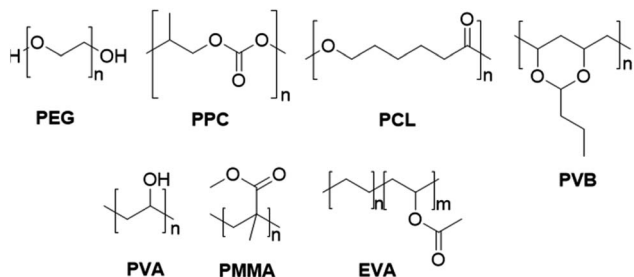
As mentioned previously, lead halide perovskite crystals (denoted as MAPbI$_3$), formed by weak ionic bonds and van der Waals interactions in their lattice structure, tend to degrade under various stimuli,[14,15] such as a strong electric field, light illumination and high temperature in a real outdoor application. To solve this issue, different approaches were used to tackle the problem, including interface engineering,[16–18] introducing ionic liquid additives,[19–21] solvent engineering,[22–24] developing new charge transport materials,[25,26] *etc.* Small molecules, such as *N*-benzyloxycarbonyl-D-valine (NBDV)[27] and D-4-*tert*-butylphenylalanine (D4TBP),[28] were employed as a surface post-treatment agent in PSCs to improve the PCE and

[a]School of Chemical Engineering and Light Industry, Guangdong University of Technology, Guangzhou, 510006, China. E-mail: qdyang@gdut.edu.cn; yphuo@gdut.edu.cn

[b]School of Materials and Energy, Guangdong University of Technology, Guangzhou, 510006, China

[c]PURI Materials, 6F, Block A, Jiazhaoye Xindong Kechuang Park, 71st Zone Xindong, Baoan District, Shenzhen, China. E-mail: david_yang@purimat.com

† Electronic supplementary information (ESI) available. See DOI: https://doi.org/10.1039/d2ta09627g

This journal is © The Royal Society of Chemistry 2023

J. Mater. Chem. A, 2023, **11**, 8791–8797 | 8791

Scheme 1 Structures of polymers with functional groups utilized in PSCs.

operational stability by Zhang *et al.* and Huang *et al.* respectively, and achieve a PCE higher than 20%.

Meanwhile, molecules with functional groups, which can interact with perovskite components, are used as additives and have been proved be an effective way for preparing high-quality perovskite films and alleviating grain boundary defects, which can significantly reduce the formation of non-radiative recombination centers and can effectively inhibit ion migration. For example, Zhao *et al.* introduced 1-ethyl-3-methylimidazole trifluoroacetate (EMIMTFA, with the functional group of trifluoroacetate) as a bifocal additive to achieve multistage passivation, which could not only interact with PbI_2 to form 1D perovskite $EMMPbI_3$, but also effectively improve the photoelectric performance and long-term stability of the device, with PCE up to 22.14%.[29] Gao *et al.* reported a conjugate molecule named 4-hydroxybiphenyl substituted naphthalene-1,8-dicarboxylic group (4OH–NMI, with the functional group of carboxylic acid), which was introduced into the perovskite precursor solution and utilized as a passivator and crystal growth

controller, displaying bi-functions of improving the crystal quality of the perovskite film and passivating defects at grain boundaries and the surface.[30] These examples show that the passivation molecules with functional groups (like carboxyl, hydroxyl, *etc.*) can successfully passivate the defects by eliminating the electronic trap states.[5,31]

Fortunately, endowed with chemical versatility, polymer materials exhibit the same passivation effect as small molecule additives. Furthermore, polymer additives possess more excellent properties of water blocking, thermal resistance, and mechanical stability, which are beneficial for enhancing the operational stability of PSCs.[32] Polymers with hydroxyl groups (Scheme 1), like polyethylene glycol (PEG),[33] can form hydrogen bonds with $MAPbI_3$ and improve the crystal morphology of perovskite. In addition, a series of polymers with different functional groups, such as poly(propylene carbonate) (PPC,[34] carbonate groups), polycaprolactone (PCL,[35] carboxyl groups), polyvinyl butyral (PVB,[36] butyral groups), polyvinyl alcohol (PVA,[36] hydroxyl groups), polymethyl methacrylate (PMMA,[37] acrylate groups), poly(ethylene-*co*-vinyl acetate) (EVA,[38] acetate groups), and poly(acrylic acid) (carboxylic acid groups), were used as additives in the perovskite, respectively. All these polymers exhibited prominent passivation effects on improving the device performance and stability towards humidity, light, heat, deformation (bending), oxygen, ambient air, *etc.*

In this work, we have synthesized a polyamide acid (poly(6-FDA-*co*-AHHFP); denoted as PAA herein, Fig. 1a) by a simple one-pot method. PAA has a variety of functional groups, such as free carboxylic acid groups, hydroxyl groups, and amide groups. Carboxylic acid and hydroxyl groups could both act as Lewis base passivators to passivate the under-coordinated Pb^{2+}, thus extending the carrier lifetime and suppressing the non-radiative
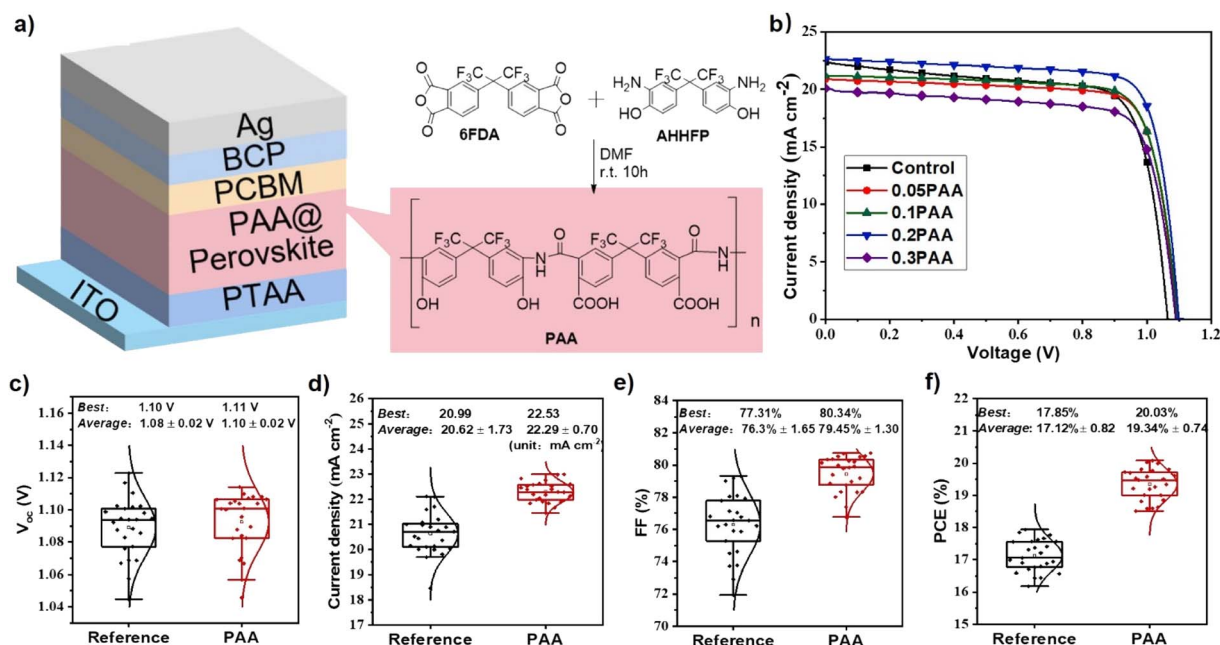

Fig. 1 (a) P–i–n type device architecture and the chemical structure and synthesize procedure of polyamide (PAA), and (b) the J–V curves for the devices with the additive PAA at a variety of concentrations (0, 0.05, 0.1, 0.2, and 0.3 mg mL^{-1}). The statistics of (c) V_{OC}; (d) J_{SC}; (e) FF; and (f) PCE of devices with and without the PAA additive.

8792 | *J. Mater. Chem. A*, 2023, **11**, 8791–8797

This journal is © The Royal Society of Chemistry 2023

recombination in the perovskite layer, ensuring the better performance of PSCs. By optimizing the concentration of PAA in the perovskite precursor solution, the champion cell shows a PCE of 20.03% with an open-circuit voltage (V_{OC}) of 1.11 V, a short-circuit current density (J_{SC}) of 22.53 mA cm^{-2}, and a fill factor (FF) of 80.34%. In sharp contrast, the PCE of the control device without additives is only 17.53%. The operational stability for the optimized device with 0.2 mg mL^{-1} PAA is also significantly improved. This study provides a versatile polymer additive treatment strategy for the preparation of efficient and stable inverted PSCs.

Results and discussion

The synthetic procedure of PAA is depicted in Fig. 1a. The crude product was obtained by introducing water into the reaction mixture, and the resulting precipitate was filtered and washed with water. The filtered powder was dried in a vacuum oven at a temperature of 60 °C overnight until yielding a dried white powder; the white powder was formed after grinding the powder and characterized by ^{1}H NMR, IR and GPC (see the ESI, Fig. S1 and S2 and Table S1†).

Our work focuses primarily on understanding the potential role of PAA in perovskite films, with a device architecture of indium tin oxide (ITO, 150 nm)/poly[bis(4-phenyl)(2,4,4-trimethylphenyl)amine] (PTAA)/PAA–methylammonium lead iodide (PAA–MAPbI$_3$)/[6,6]-phenyl C61 butyric acid methyl ester (PCBM)/bathocuproine (BCP)/silver (Ag, 100 nm). The PTAA serves as the hole transporting material and a solution with a concentration of 3.0 mg mL^{-1} was spin-coated on top of ITO glass at a spin speed of 3000 rpm s^{-1} for 30 s and annealed at 100 °C for 10 min. Then, perovskite precursor solution with different concentrations of PAA additives was spin-coated on the PTAA surface at a spin speed of 4000 rpm s^{-1} for 30 s and then annealed at 100 °C for 10 min. Subsequently, the electron transporting layer PCBM and interface layer BCP were spin-coated from their chlorobenzene and isopropanol solution layer by layer, respectively. Finally, a silver electrode was prepared by

thermal evaporation to finish the device fabrication. The device architecture and PAA synthetic procedure are shown in Fig. 1a. After optimizing the concentration, a device with a PAA concentration of 0.2 mg mL^{-1} displays the best performance. The device performances are summarized in Table 1 and the corresponding J–V curves are also exhibited in Fig. 1b, respectively. It can be clearly seen that the 0.2 mg mL^{-1} PAA passivated device (denoted as 0.2PAA) displays a champion PCE of 20.03% with a high V_{OC} of 1.11 V, J_{SC} of 22.53 mA cm^{-2}, and FF of 80.34%, which are better than those of the control device (PCE of 17.00%, V_{OC} of 1.08 V, J_{SC} of 21.03 mA cm^{-2} and FF of 74.89%). However, with further increasing the content of PAA in perovskite precursor solution to 0.3 mg mL^{-1}, the PCE dramatically drops to 15.44%, due to the insulating properties of PAA. Excellent reproducibility can be found from the statistical parameters from 25 devices for both 0.2PAA and the control devices, as shown in Fig. 1c–f. 0.2PAA passivated devices display much higher average efficiencies than the control ones, which can be ascribed to the improved J_{SC} and FF. The improved J_{SC} can be correlated with an improved absorbance (Fig. 2c), which is likely due to an enhanced light scattering by the larger grain size.[34]

To prove that the enhancement in solar cell effects results from the polymer PAA, the addition of PAA's monomers, 6FDA and AHHFP, as additives into the fabrication of PSCs was also examined (see Fig. S3 in the ESI†). It is clearly seen that PAA shows greater improvement in PCE than applying only one of these monomers.

It is reported that ion migration is a primary reason for device hysteresis.[39–42] The additive PAA, functionalized with sufficient sub-branches of hydroxyl groups and carboxylic groups, will immobilize the lead ions, thus alleviating device hysteresis. This passivation effect of the PAA additive could be observed from the J–V curves with forward and reverse scans shown in Fig. 2a. Here we use the hysteresis index (HI = |PCE$_{reverse}$ − PCE$_{forward}$|/PCE$_{reverse}$ × 100%) to determine the degree of hysteresis. The PSCs with the 0.2PAA additive have a low HI of 2.5%, while the control device has a relatively higher value of 3.1% (calculated from Table 1). Compared to the perovskite film with the 0.2PAA additive, the control film might exhibit a severe organic cation-deficient perovskite system, and would contain ionic defects, that can screen the external bias, which is a common reason for enlarged current–voltage hysteresis.[43]

The EQE spectra of these devices were also recorded. As shown in Fig. 2b, it can be observed that the EQE response of the PAA passivated device is higher than that of the control device, corresponding well with the higher J_{SC} of the PAA passivated device. The integrated current densities calculated from EQE spectra are 21.53 and 21.27 mA cm^{-2} for control and PAA passivated devices, respectively, which are well consistent with the J–V curves. As shown in Fig. 2c, the light absorbance of the perovskite film with the PAA additive is slightly stronger than that of the pristine film. This indicates that the addition of a moderate amount of PAA can enhance the optical absorption intensity, which is a benefit for achieving a high J_{SC} and thus

Table 1 Summary of the photovoltaic parameters for the PSCs without and with PAA with different concentrations^a

		V_{OC} (V)	J_{SC} (mA cm^{-2})	PCE (%)	FF (%)
Control	FW	1.06	22.35	17.53	73.68
	RS	1.08	21.03	17.00	74.89
0.05PAA	FW	1.09	20.88	17.89	78.39
	RS	1.09	20.00	17.53	80.48
0.1PAA	FW	1.10	21.17	18.06	77.83
	RS	1.09	21.00	17.81	77.40
0.2PAA	FW	1.10	22.63	19.52	78.43
	RS	1.11	22.53	20.03	80.34
0.3PAA	FW	1.09	20.06	16.45	75.28
	RS	1.08	18.17	15.44	78.81

^{a} Additive PAA in the perovskite film is fabricated by spin coating of a solution with an admixture of PAA with specified concentrations (0.05 mg mL^{-1}, 0.1 mg mL^{-1}, 0.2 mg mL^{-1} and 0.3 mg mL^{-1}) into a precursor perovskite solution (MAPbI$_3$). And they are denoted as 0.05PAA, 0.1PAA, 0.2PAA and 0.3PAA, respectively.
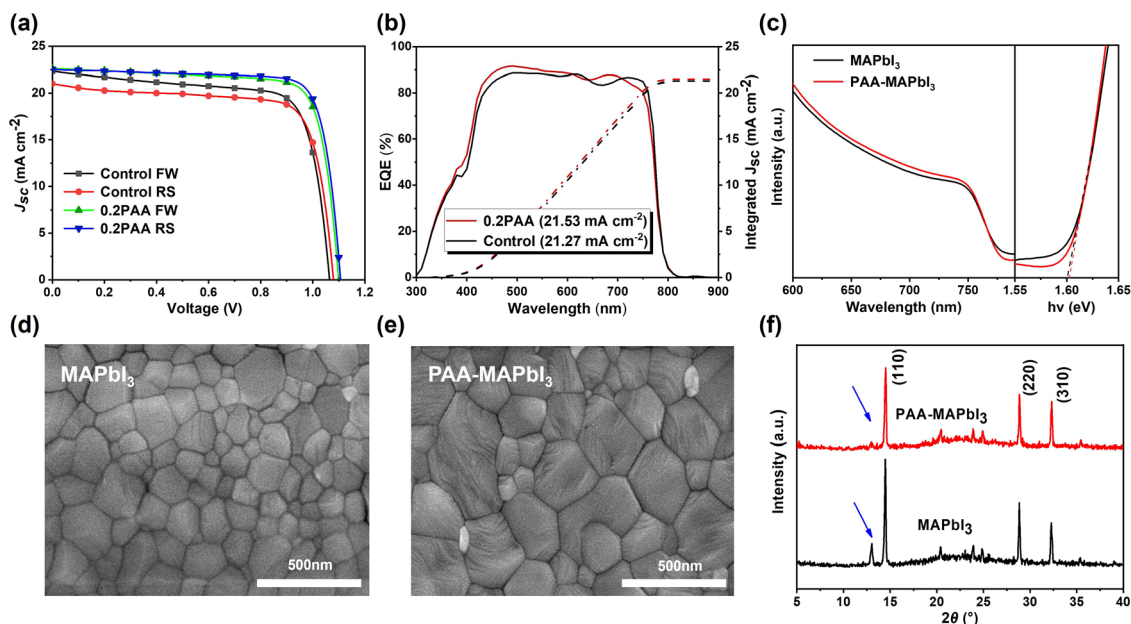
This journal is © The Royal Society of Chemistry 2023

J. Mater. Chem. A, 2023, **11**, 8791–8797 | **8793**

Fig. 2 (a) J–V curves; (b) EQE spectra and integrated J_{SC} value *versus* the wavelength of light for the devices with/without 0.2PAA. (c) Left, UV-Vis absorption spectra; and right, Tauc's plot; top-view SEM images of the perovskite film (d) without and (e) with 0.2PAA passivation; (f) XRD patterns.

improving the performance of PSCs. This result is consistent with the J–V curve shown in Fig. 1a.

Scanning electron microscope (SEM) images of $MAPbI_3$ with and without PAA are recorded to distinguish the effect of PAA on the film morphology. As shown in Fig. 2d and e, the neat $MAPbI_3$ film displays a large number of small-size grain crystals in the range of 100 to 200 nm, while the crystals for PAA passivated films have obviously increased in the range of 300–400 nm. The increased crystal sizes indicate that the number of grain boundaries was dramatically reduced, which is a benefit for reducing defect density in perovskite films. At the same time, the film with a larger grain size can help the device achieve better performance and stability. The X-ray diffraction (XRD) patterns of the perovskite films were examined to study the crystallinity variation by the introducing of the PAA additive (Fig. 3f). It can be seen that both samples show similar diffraction peaks at 14.1, 28.4 and 31.8°, which can be assigned to the (110), (220), and (310) crystal faces of tetragonal $MAPbI_3$, respectively.[44] There is no difference that can be observed in the crystal structure, which indicates that PAA molecules cannot embed in the perovskite crystal lattice and can only locate at the surface or ground boundaries. Interestingly, a diffraction peak located at 13.4°, which can be assigned to PbI_2, was diminished for the perovskite film with the PAA additive, suggesting that PAA can interact with perovskite components and inhibit the organic cation escape from the perovskite crystal during thermal annealing.

To clarify the origin of improved performance for PAA passivated devices, steady-state photoluminescence (PL) spectra and time-resolved PL (TRPL) spectra are recorded and the spectra are shown in Fig. 3a. The fitted parameters of the TRPL curves are summarized in the inserted table. The peak positions

for steady-state PL spectra did not show noticeable change, indicating that the functional groups in PAA did not affect the optical bandgap of perovskite. Notably, the PL intensity for $MAPbI_3$ films with PAA is much higher than that of the pristine film, demonstrating that the O–H and COOH groups can passivate defects in the perovskite film. To study the influence of PAA on the charge-transfer dynamic between the $MAPbI_3$ film and PTAA, steady-state PL spectra were also recorded for $MAPbI_3$ films with and without PAA on the PTAA film on an ITO glass substrate (the left curves in Fig. 3b). The steady-state PL intensity of the perovskite with the 0.2PAA additive on PTAA was largely reduced compared to the bare perovskite film. This suggests that the PAA additive could assist PTAA in extracting charge carriers from the perovskite film more efficiently, which is consistent with the higher FF and less hysteresis.[43] TRPL was also measured to compare the trap density of perovskite films with and without the PAA additive. Fig. 3b shows the TRPL of perovskite films on glass, the measured data were fitted with a bi-exponential decay model and the detailed parameters are summarized in the table inserted in Fig. 3b. For the bi-exponential decay model, the faster decay components are attributed to the defect-assisted non-radiative recombination, and the slower decay components are assigned to bimolecular radiative recombination in the bulk.[20] The film with the PAA additive exhibited an increased fast-decay lifetime τ_1 of 86.19 ns, compared to that of the control $MAPbI_3$ film of 10.22 ns. Moreover, the slow-decay lifetime τ_2 was also extended, from 51.72 ns (pristine perovskite film) to 166.9 ns (PAA passivated perovskite film), demonstrating a longer charge carrier lifetime within the bulk films. The increased lifetime suggests a lower defect density of the film, which mainly originates from two

8794 | *J. Mater. Chem. A*, 2023, **11**, 8791–8797

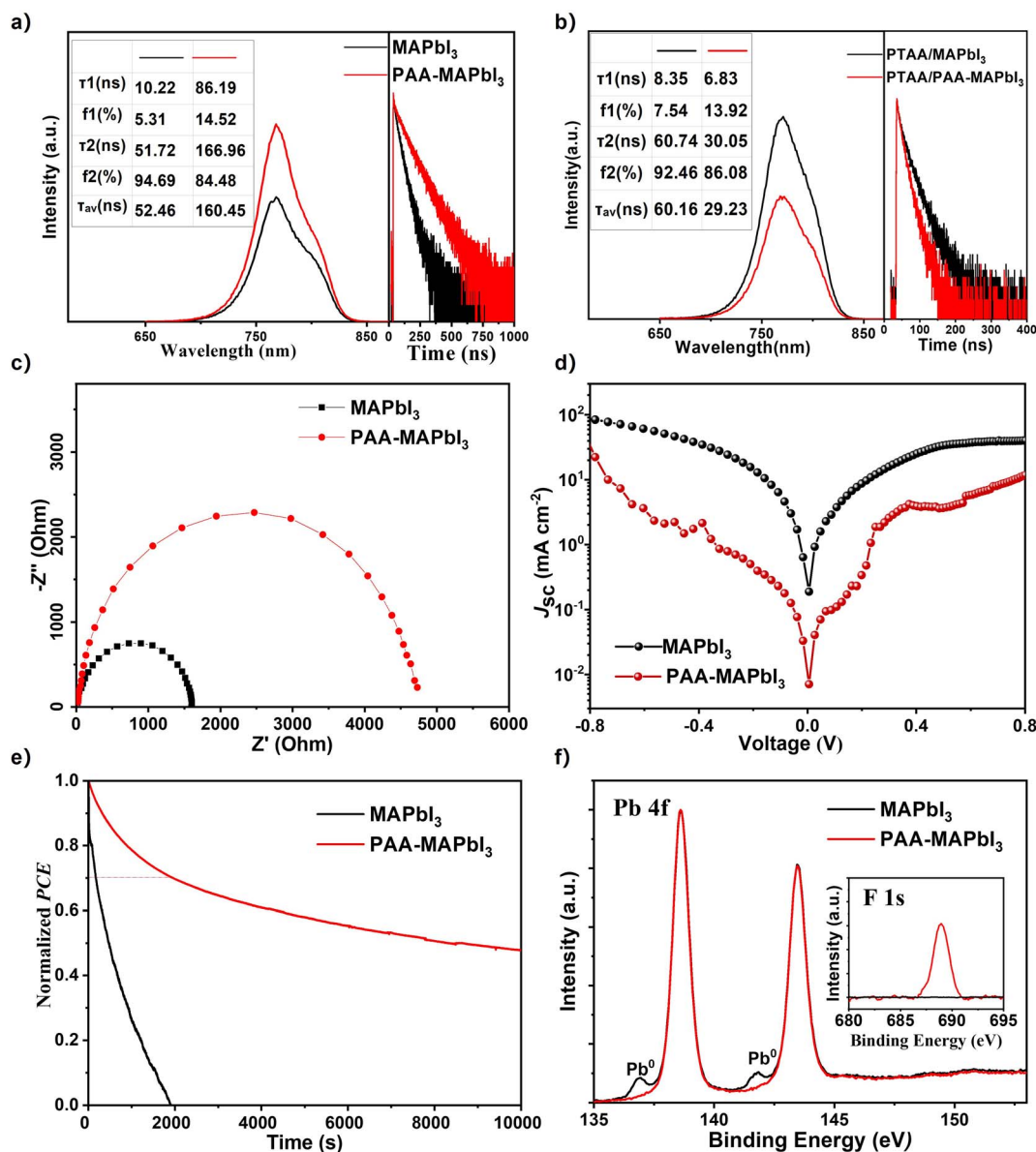This journal is © The Royal Society of Chemistry 2023

Fig. 3 (a) Steady-state PL spectra and time-resolved PL spectra (inset table shows the fitted parameters of TRPL curves) of perovskite films with/without PAA, and the same group (b) coating on the PTAA film; (c) ESI and (d) J−V characteristics of devices with and without PAA in the dark. (e) Enduring stability showing the PCE at a fix MPP voltage as a function of time at room temperature; (f) high resolution XPS spectra of Pb (in the inset, the curve is F 1s XPS spectra).

factors, reduced grain boundaries due to the increased grain sizes and efficient passivation by the PAA additive.

To study the effect of the introduction of PAA on the charge transport process, electrochemical impedance spectroscopy (EIS) was carried out as shown in Fig. 3c. The measurement was performed with a bias potential of 0.9 V under dark conditions in the frequency range of 10^6 to 0.01 Hz. It is well known that the semicircle in the low-frequency range represents the recombination resistance.[19] It can be seen from the Nyquist diagram that the recombination resistance is much larger for the PAA passivated device than that of the reference device. A larger recombination resistance indicates that the trap-state density in the perovskite layer decreases and the polymer PAA can

effectively inhibit charge recombination, thus leading to the improvement of photovoltaic performance. In addition, the dark current measurement in Fig. 3d also confirmed the suppressed charge carrier recombination. The dark current density of the control device was nearly more than one order of magnitude higher than that of the PAA passivated device, indicating that more photocurrents were shunted. The PAA-based device inhibited charge carrier recombination and leakage current. And these are consistent with the PL and TRPL measurements.

Accordingly, it is proved that the hysteresis problem is alleviated by the PAA additive. To study the influence of PAA on the stability of PSCs, stability testing for devices with and without

This journal is © The Royal Society of Chemistry 2023

J. Mater. Chem. A, 2023, **11**, 8791–8797 | **8795**

the PAA additive was also carried out. As shown in Fig. 3e, the 0.2PAA passivated devices show a significant improvement in stability and the data are tracked from the maximum power point (MPP) at room temperature (25 °C). The PCE of the 0.2PAA passivated device can remain at its initial value of 70% after the device operation at the maximum power point (MPP) voltage for 2000 s, while the control one dramatically drops to zero in 1900 s. This is attributed to the reduction of trap density and ion migration in the perovskite layer. In perovskite films, grain boundaries serve as the penetration channels for moisture, oxygen from the ambient atmosphere and the degradation usually starts from the grain boundaries and then spread to the whole films.[44] The solution process fabricated perovskite films are polycrystalline and the grain boundaries are inevitable and always exist. Thus, it is necessary to well manipulate the grain boundaries in perovskite films to achieve stable PSCs. In our work, we use polymer PAA with functional groups of carboxyl and hydroxyl as an additive to interact with perovskite components and promote the formation of large grain sizes, which can dramatically decrease the number of grain boundaries. The results match well with the SEM images as shown in Fig. 2d and e. In addition, the contact angle was used to further investigate the effect of PAA on the stability of PSCs. As shown in Fig. S4,† the contact angle of the perovskite film with the PAA additive is increased from 31.8° to 41.8°, which is mainly due to the hydrophobic groups of trifluoromethyl in PAA.

To investigate the interaction between $MAPbI_3$ and PAA, the $MAPbI_3$ film was characterized by X-ray spectroscopy (XPS). As shown in Fig. 3f, the high-resolution XPS spectra of Pb 4f for perovskite films with and without PAA were recorded. There are two main peaks located at 138.6 and 143.5 eV, which can be assigned to Pb 4f 7/2 and Pb 4f 5/2, respectively. However, for the film without the PAA additive, two additional peaks located at 136.9 and 141.7 eV can be observed, which can be ascribed to metallic lead on the perovskite film surface.[45] The appearance of metallic lead may be caused by the iodine and organic cation vacancies.[46,47] The peak intensity of metallic lead is dramatically reduced by introducing the PAA additive, indicating the preserved number of organic cations and reduced under-coordinated lead atoms. To verify the existence of PAA in the perovskite film, the XPS spectra of F 1s for perovskite films with and without the PAA additive were recorded shown as the inset spectra in Fig. 3f. The peak located at 688.9 eV is attributed to the signal of F 1s, which comes from the functional group of PAA, indicating that the PAA has been incorporated into the perovskite bulk successfully. Simultaneously, ultraviolet-visible (UV-Vis) absorption spectra were recorded to investigate the influence of the PAA additive on the optical properties of the perovskite film. In order to further elucidate the interaction between PAA and precursors in perovskite, PAA was added into the MAI and PbI_2 solution respectively. As shown in the photographs in Fig. S5 (in the ESI†), the transparent MAI solution tunned light yellow after PAA was added, which indicated a strong interaction between PAA and MAI molecules. According to the literature, we speculated that fluoro groups in PAA could interact with methyl ammonium cations to form hydrogen bonds and provide immobility of monovalent cations.

In addition, the carbonyl groups could bond with under-coordinated Pb^{2+} and passivate the surface. Furthermore, the CF_3 groups in PAA will also increase the hydrophobicity of the perovskite surface, acting as a barrier to slow down the degradation of perovskite crystals during expose to moisture.

Conclusions

In conclusion, we have used a simple and convenient one-pot method to synthesize polymer PAA under room temperature. After that, PAA was employed as an additive in the perovskite precursor solution and exhibited multiple effects, including enlarging perovskite crystal grain sizes, and enhancing light absorption and charge transfer. In addition, PAA was also adopted to prevent the surface cations from escaping from the perovskite film surface during the thermal annealing process and guarantee the stoichiometric balance of the perovskite. An optimized concentration of 0.2PAA in the perovskite film was achieved and the corresponding PSCs showed an efficiency of 20.03% with less hysteresis. At the same time, the device with PAA showed an obviously enhanced operational stability. This work provides a cheap and effective passivation polymer used as an additive in PSCs to improve both performance and operational stability.

Author contributions

H. Luo designed the research and conducted all the experiments, and prepared the manuscript. F. Tu synthesized the PAA polymer. X. Chen contributed to the SEM characterization. L. Xing carried out the TRPL measurements. L. Cao carried out the XRD measurements. G. Ren carried out the EQE measurements. S. Ji, Y. Zhong and W.-C. Chen revised the manuscript. Q.-D. Yang, C. Yang and Y. Huo revised the manuscript and supervised the entire process of the project.

Conflicts of interest

There are no conflicts to declare.

Acknowledgements

Notes and references

1 P. Liu, W. Wang, S. Liu, H. Yang and Z. Shao, *Adv. Energy Mater.*, 2019, **9**, 1803017.

2 X. Wu, L. Zhang, Z. Xu, S. Olthof, X. Ren, Y. Liu, D. Yang, F. Gao and S. Liu, *J. Mater. Chem. A*, 2020, **8**, 8313.

3 L. Chu, S. Zhai, W. Ahmad, J. Zhang, Y. Zang, W. Yan and Y. Li, *Nano Energy*, 2022, **1**, 9120024.

8796 | *J. Mater. Chem. A*, 2023, **11**, 8791–8797

This journal is © The Royal Society of Chemistry 2023

4 J. Jiang, J. M. Vicent-Luna and S. Tao, *J. Energy Chem.*, 2022, **68**, 393.

5 A. Rajagopal, Z. Yang, S. B. Jo, I. L. Braly, P. W. Liang, H. W. Hillhouse and A. K. Jen, *Adv. Mater.*, 2017, **29**, 1702140.

6 A. Kojima, K. Teshima, Y. Shirai and T. Miyasaka, *J. Am. Chem. Soc.*, 2009, **131**, 6050.

7 C. C. Boyd, R. Cheacharoen, T. Leijtens and M. D. McGehee, *Chem. Rev.*, 2019, **119**, 3418.

8 G. Y. Kim, A. Senocrate, T. Y. Yang, G. Gregori, M. Gratzel and J. Maier, *Nat. Mater.*, 2018, **17**, 445.

9 T. Supasai, N. Rujisamphan, K. Ullrich, A. Chemseddine and T. Dittrich, *Appl. Phys. Lett.*, 2013, **103**, 4826116.

10 Q. Yao, Q. Xue, Z. Li, K. Zhang, T. Zhang, N. Li, S. Yang, C. J. Brabec, H. L. Yip and Y. Cao, *Adv. Mater.*, 2020, **32**, e2000571.

11 Y. Cheng and L. Ding, *Energy Environ. Sci.*, 2021, **14**, 3233–3255.

12 M. Kim, S. G. Motti, R. Sorrentino and A. Petrozza, *Energy Environ. Sci.*, 2018, **11**, 2609.

13 J. Tian, Q. Xue, X. Tang, Y. Chen, N. Li, Z. Hu, T. Shi, X. Wang, F. Huang, C. J. Brabec, H. L. Yip and Y. Cao, *Adv. Mater.*, 2019, **31**, e1901152.

14 J. Kim, A. Ho-Baillie and S. J. Huang, *Sol. RRL*, 2019, **3**, 1800302.

15 W. Chen, X. Li, Y. Li and Y. Li, *Energy Environ. Sci.*, 2020, **13**, 1971.

16 P. L. Qin, G. Yang, Z. W. Ren, S. H. Cheung, S. K. So, L. Chen, J. Hao, J. Hou and G. Li, *Adv. Mater.*, 2018, **30**, e1706126.

17 C. Liu, J. Zhang, L. Zhang, X. Zhou, Y. Liu, X. Wang and B. Xu, *Adv. Energy Mater.*, 2022, **12**, 2200945.

18 N. K. Noel, S. N. Habisreutinger, A. Pellaroque, F. Pulvirenti, B. Wenger, F. Zhang, Y.-H. Lin, O. G. Reid, J. Leisen, Y. Zhang, S. Barlow, S. R. Marder, A. Kahn, H. J. Snaith, C. B. Arnold and B. P. Rand, *Energy Environ. Sci.*, 2019, **12**, 3063.

19 X. Xia, J. Peng, Q. Wan, X. Wang, Z. Fan, J. Zhao and F. Li, *ACS Appl. Mater. Interfaces*, 2021, **13**, 17677.

20 H. Zeng, L. Li, F. Liu, M. Li, S. Zhang, X. Zheng, L. Luo, S. You, Y. Zhao, R. Guo, Z. Gong, R. Huang, Z. Li, T. Wang, Y. Cui, Y. Rong and X. Li, *Adv. Energy Mater.*, 2021, **12**, 2102820.

21 Y. Wu, Q. Wang, Y. Chen, W. Qiu and Q. Peng, *Energy Environ. Sci.*, 2022, **15**, 4700.

22 H. Zhang, K. Darabi, N. Y. Nia, A. Krishna, P. Ahlawat, B. Guo, M. H. S. Almalki, T. S. Su, D. Ren, V. Bolnykh, L. A. Castriotta, M. Zendehdel, L. Pan, S. S. Alonso, R. Li, S. M. Zakeeruddin, A. Hagfeldt, U. Rothlisberger, A. Di Carlo, A. Amassian and M. Gratzel, *Nat. Commun.*, 2022, **13**, 89.

23 G. Li, J. Song, J. Wu, Z. Song, X. Wang, W. Sun, L. Fan, J. Lin, M. Huang, Z. Lan and P. Gao, *ACS Energy Lett.*, 2021, **6**, 3614–3623.

24 Y. Yu, R. Liu, C. Liu, X. L. Shi, H. Yu and Z. G. Chen, *Adv. Energy Mater.*, 2022, **12**, 2201509.

25 Y. Bai, Z. Zhou, Q. Xue, C. Liu, N. Li, H. Tang, J. Zhang, X. Xia, J. Zhang, X. Lu, C. J. Brabec and F. Huang, *Adv. Mater.*, 2022, **34**, e2110587.

26 T. Niu, W. Zhu, Y. Zhang, Q. Xue, X. Jiao, Z. Wang, Y.-M. Xie, P. Li, R. Chen, F. Huang, Y. Li, H.-L. Yip and Y. Cao, *Joule*, 2021, **5**, 249.

27 J. Xiong, N. Liu, X. Hu, Y. Qi, W. Liu, J. Dai, Y. Zhang, Z. Dai, X. Zhang, Y. Huang, Z. Zhang, Q. Dai and J. Zhang, *Adv. Energy Mater.*, 2022, **12**, 2201787.

28 S. Yang, J. Dai, Z. Yu, Y. Shao, Y. Zhou, X. Xiao, X. C. Zeng and J. Huang, *J. Am. Chem. Soc.*, 2019, **141**, 5781.

29 N. Wei, Y. Chen, X. Wang, Y. Miao, Z. Qin, X. Liu, H. Wei and Y. Zhao, *Adv. Funct. Mater.*, 2021, **32**, 2108944.

30 Z. Zhang, Y. Gao, Z. Li, L. Qiao, Q. Xiong, L. Deng, Z. Zhang, R. Long, Q. Zhou, Y. Du, Z. Lan, Y. Zhao, C. Li, K. Mullen and P. Gao, *Adv. Mater.*, 2021, **33**, e2008405.

31 I. L. Braly, D. W. deQuilettes, L. M. Pazos-Outón, S. Burke, M. E. Ziffer, D. S. Ginger and H. W. Hillhouse, *Nat. Photonics*, 2018, **12**, 355.

32 S. Collavini, A. Cabrera-Espinoza and J. L. Delgado, *Macromolecules*, 2021, **54**, 5451.

33 Y. Zhao, J. Wei, H. Li, Y. Yan, W. Zhou, D. Yu and Q. Zhao, *Nat. Commun.*, 2016, **7**, 10228.

34 T. H. Han, J. W. Lee, C. Choi, S. Tan, C. Lee, Y. Zhao, Z. Dai, N. De Marco, S. J. Lee, S. H. Bae, Y. Yuan, H. M. Lee, Y. Huang and Y. Yang, *Nat. Commun.*, 2019, **10**, 520.

35 Y. Lan, Y. Wang and Y. Song, *Flexible Printed Electron.*, 2020, **5**, 1.

36 D. Wang, L. Zhang, K. M. Deng, W. N. Zhang, J. Song, J. H. Wu and Z. Lan, *Energy Technol.*, 2018, **6**, 2380.

37 Y. Yue, T. Umeyama, Y. Kohara, H. Kashio, M. Itoh, S. Ito, E. Sivaniah and H. Imahori, *J. Phys. Chem. C*, 2015, **119**, 22847.

38 Z. Huang, X. Hu, C. Liu, X. Meng, Z. Huang, J. Yang, X. Duan, J. Long, Z. Zhao, L. Tan, Y. Song and Y. Chen, *Adv. Funct. Mater.*, 2019, **29**, 1902629.

39 Q. Jiang, J. Tong, Y. Xian, R. A. Kerner, S. P. Dunfield, C. Xiao, R. A. Scheidt, D. Kuciauskas, X. Wang, M. P. Hautzinger, R. Tirawat, M. C. Beard, D. P. Fenning, J. J. Berry, B. W. Larson, Y. Yan and K. Zhu, *Nature*, 2022, **611**, 278.

40 A. N. Singh, S. Kajal, J. Kim, A. Jana, J. Y. Kim and K. S. Kim, *Adv. Energy Mater.*, 2020, **10**, 2000768.

41 L. K. Ono, S. F. Liu and Y. Qi, *Angew. Chem., Int. Ed.*, 2020, **59**, 6676.

42 Y. Chen, W. Zhou, X. Chen, X. Zhang, H. Gao, N. A. N. Ouedraogo, Z. Zheng, C. B. Han, Y. Zhang and H. Yan, *Adv. Funct. Mater.*, 2021, **32**, 2108417.

43 L. Meng, C. Sun, R. Wang, W. Huang, Z. Zhao, P. Sun, T. Huang, J. Xue, J. W. Lee, C. Zhu, Y. Huang, Y. Li and Y. Yang, *J. Am. Chem. Soc.*, 2018, **140**, 17255.

44 X. Li, W. Zhang, W. Zhang, H.-Q. Wang and J. Fang, *Nano Energy*, 2019, **58**, 825.

45 L. Lee, J. Baek, K. S. Park, Y. E. Lee, N. K. Shrestha and M. M. Sung, *Nat. Commun.*, 2017, **8**, 15882.

46 H. Choi, X. Liu, H. I. Kim, D. Kim, T. Park and S. Song, *Adv. Energy Mater.*, 2021, **11**, 2003829.

47 B. Chen, P. N. Rudd, S. Yang, Y. Yuan and J. Huang, *Chem. Soc. Rev.*, 2019, **48**, 3842.

This journal is © The Royal Society of Chemistry 2023

J. Mater. Chem. A, 2023, **11**, 8791–8797 | **8797**